Molecular Cell, Vol. 4, 85–95, July, 1999, Copyright ©1999 by Cell Press

Crystal Structure of the Vesicular Transport Protein Sec17: Implications for SNAP Function in SNARE Complex Disassembly

Luke M. Rice and Axel T. Brunger*
The Howard Hughes Medical Institute and
Department of Molecular Biophysics and Biochemistry
Yale University
New Haven, Connecticut 06520

Summary

SNAP proteins play an essential role in membrane trafficking in eukaryotic cells. They activate and recycle SNARE proteins by serving as adaptors between SNAREs and the cytosolic chaperone NSF. We have determined the crystal structure of Sec17, the yeast homolog of α-SNAP, to 2.9 Å resolution. Sec17 is composed of an N-terminal twisted sheet of α-helical hairpins and a C-terminal α-helical bundle. The N-terminal sheet has local similarity to the tetratricopeptide repeats from protein phosphatase 5 but has a different overall twist. Sec17 also shares structural features with HEAT and clathrin heavy chain repeats. Possible models of SNAP:SNARE binding suggest that SNAPs may function as lever arms, transmitting forces generated by conformational changes in NSF/Sec18 to drive disassembly of SNARE complexes.

Introduction

Membrane trafficking in eukaryotic cells is a highly regulated process essential for diverse processes, including maintenance of distinct subcellular compartments, protein and hormone secretion, and neurotransmitter release (reviewed in Rothman, 1994; Schekman and Orci, 1996). Many intracellular fusion events use a common, evolutionarily conserved protein machinery (Ferro-Novick and Jahn, 1994) that includes the hexameric ATPase NSF (N-ethylmaleimide-sensitive factor, Sec18 in yeast) (Eakle et al., 1988; Malhotra et al., 1988; Graham and Emr, 1991) and its adaptor, SNAP (soluble NSF attachment protein, Sec17 in yeast) (Clary et al., 1990; Griff et al., 1992). NSF/Sec18 and SNAP act together in membrane fusion events of many different types, ranging from the homotypic fusion between vacuole-derived vesicles in yeast (Haas and Wickner, 1996) to the fusion of synaptic vesicles with the presynaptic plasma membrane in neurons (Söllner et al., 1993). Integral membrane SNAP receptor (SNARE) proteins can form both *cis* (same membrane) and *trans* (opposing membranes) complexes that are substrates for SNAPs and NSF (Otto et al., 1997; Ungermann et al., 1998). *Trans* SNARE complexes play an important role in vesicle fusion (Ungermann et al., 1998; Chen et al., 1999). Liposome fusion experiments suggested that SNARE proteins can act as the minimal fusion machinery (Weber et al., 1998), but studies of vacuole fusion suggested that downstream effectors may also be required (Ungermann et al., 1998). Fusion of opposing membranes results in the formation of *cis* SNARE complexes that are disassembled for recycling and reactivation by the joint action of SNAP and NSF/Sec18.

SNAP and NSF/Sec18 bind sequentially to SNARE complexes, forming 20S particles. In vitro reconstitution of the fusion between yeast vacuole-derived vesicles has shown that the requirement for the activity of Sec18 (NSF) and Sec17 (SNAP) can be fulfilled prior to vesicle docking (Mayer et al., 1996). SNAPs and NSF act promiscuously at many different transport stages, but SNARE proteins appear to be specialized for specific transport stages (Ferro-Novick and Jahn, 1994; Yang et al., 1999). Limited proteolysis and biophysical studies of SNARE complexes (Fasshauer et al., 1998a; Poirier et al., 1998; Fiebig et al., 1999) have been used to identify a minimal core of the SNARE complex necessary and sufficient for assembly and disassembly. The crystal structure of the synaptic minimal core complex consists of a parallel four-helix bundle (Sutton et al., 1998).

Interactions between SNAPs and SNAREs have primarily been mapped using deletion mutagenesis and in vitro binding studies. The SNAP-interacting region of SNAREs overlaps with their core complex–forming regions (Hanson et al., 1995; Hayashi et al., 1995; Kee et al., 1995). This, in conjunction with the structure of the synaptic core complex (Sutton et al., 1998) and the observed promiscuity of SNAP:SNARE interactions, suggests that SNAPs recognize general surface features (shape or electrostatic charge distribution) of the parallel four-helix bundle. Experiments aimed at determining the minimal SNARE-interacting portion of α-SNAP showed that the 63 N-terminal and the 37 C-terminal residues of α-SNAP were essential for binding to the ternary SNARE complex (Hayashi et al., 1995). Subsequent electron microscopy studies of SNAP:SNARE complexes show that SNAP appears to "coat" the SNARE complex along most of its length (Hohl et al., 1998).

Interactions between Sec17/SNAP and Sec18/NSF have also been characterized. The N-terminal domain of NSF (Tagaya et al., 1993) is essential for the interaction between NSF, SNAP, and SNAREs (Nagiec et al., 1995). In general, Sec17/SNAP and Sec18/NSF only bind to each other if SNAREs also bind, or if SNAP is bound to a plastic surface (Clary et al., 1990). This may be due to a conformational change in SNAP induced upon binding either to SNAREs or to a plastic surface (Whiteheart et al., 1992). The extreme C-terminal residues of α-SNAP play a key role in stimulating the ATPase activity of NSF (Barnard et al., 1997). Finally, both N- and C-terminal fragments (1–160 and 160–295) of α-SNAP are able to bind NSF (Barnard et al., 1997), but it has not been shown that these truncations were properly folded.

In order to better understand the mechanism of SNAP function in NSF/Sec18-mediated SNARE complex disassembly, we have determined the structure of a yeast SNAP, Sec17. The structure of Sec17 reported here allows detailed structural examination of a SNAP protein. Sec17 adopts a fold primarily composed of α-helical hairpins. The structure of Sec17 shows unexpected local similarity to several other α/α structures known to mediate protein–protein interactions as part of larger

*To whom correspondence should be addressed (e-mail: brunger@laplace.csb.yale.edu).

Table 1. Crystallographic Data, Phasing, and Refinement

Crystallographic Data

	a (Å)	b (Å)	c (Å)	d_{min} (Å)	Number of Unique Reflections	Redundancy	Completeness (%)	I/σ	R_{sym}[a] (%)
Native (0.979 Å)	107.9	107.9	46.1	2.9	11,999	3.9 (3.7)	99.9 (99.3)	23.6 (4.0)	5.4 (47.2)
Se–Met λ_1 (0.98 Å)	108.2	108.2	46.5	3.3	15,743	3.9 (3.8)	99.8 (99.9)	18.7 (5.1)	7.0 (31.3)
Se–Met λ_2 (0.9802 Å)	108.2	108.2	46.5	3.3	15,769	3.9 (3.8)	99.9 (100.0)	18.1 (4.3)	7.7 (37.6)

Observed Diffraction Ratios[b]

	λ_1	λ_2
λ_1	0.048	0.055
λ_2		0.037

Phasing Power[c] and Figure of Merit (FOM)

	Phasing Power	FOM
15–3.8 Å	0.99	0.2
3.96–3.8 Å	0.22	0.05

Overall figure of merit after density modification and phase extension: 0.85

Refinement

Resolution (Å)	Overall (500–2.9 Å)	500–6.25	4.96	4.33	3.94	3.65	3.44	3.27	3.12	3.00	2.90
R value[d]	25.9	22.2	27.0	18.6	20.1	25.1	29.0	34.0	35.7	40.9	45.2
R_{free}[e]	28.2	24.8	31.6	20.1	21.6	27.8	30.5	35.8	39.3	43.9	51.0
Luzzati coordinate error	0.49 Å										
Cross-validated Luzzati coordinate error	0.54 Å										
Bond length deviation	0.009 Å										
Bond angle deviation	1.3°										
Improper angle deviation	0.72°										
Dihedrals	18.2°										
Average B factor	67.7 Å^2										
Rmsd for bonded main chain atoms	2.46 Å^2										
Rmsd for bonded side chain atoms	4.01 Å^2										
Minimum B factor	32.4 Å^2										
Maximum B factor	151.3 Å^2										
Residues in core ϕ–ψ region (%)	81.4%										
Residues in disallowed regions (%)	0.0%										

Values in parentheses are for the high-resolution bin.

[a] $R_{sym} = \Sigma_h\Sigma_i|I_i(h) - \langle I(h)\rangle|/\Sigma_h\Sigma_i I_i(h)$, where $I_i(h)$ is the i^{th} measurement and $\langle I(h)\rangle$ is the mean of all measurements of I(h) for Miller indices h.

[b] Values are $\langle(\Delta|F|)^2\rangle^{1/2}/\langle|F|^2\rangle^{1/2}$, where $\Delta|F|$ is the dispersive (off-diagonal element), or Bijvoet difference (diagonal elements), computed between 15 and 3.8 Å resolution.

[c] SAD phasing power is defined as $[\langle\,|F^+| - |F^-|\,|^2\rangle/\int_\phi P(\phi)(|F^-|e^{i\phi}+\Delta F|-|F^+|)^2 d\phi]^{1/2}$, where $P(\phi)$ is the experimental phase probability distribution. F^+ and F^- correspond to a Bijvoet pair of structure factors, and ΔF is the difference in the heavy atom structure factor.

[d] $R = \Sigma(|F_{obs}| - k|F_{calc}|)/\Sigma|F_{obs}|$.

[e] Free R value is the R value obtained for a test set of reflections, consisting of a randomly selected 10% subset of the diffraction data, not used during refinement.

assemblies: TPRs (Das et al., 1998), 14-3-3 (Yaffe et al., 1997), HEAT repeats (Groves et al., 1999), and clathrin heavy chain repeats (Ybe et al., 1999). A molecular understanding of the mechanism of SNARE complex disassembly is now closer at hand, because structures of most of the individual components of a 20S NSF: SNAP:SNARE complex have now been determined, namely SNAP/Sec17, the core synaptic SNARE complex (Sutton et al., 1998), the D2 oligomerization domain of NSF (Lenzen et al., 1998; Yu et al., 1998), and the structure of the N-terminal SNARE-binding domain of NSF (Yu et al., 1999 [this issue of *Molecular Cell*]).

Results and Discussion

Structure Determination

Crystals of recombinantly expressed Sec17 were initially obtained at 4°C by hanging drop vapor diffusion using a polyethyleneimine condition derived from sparse matrix screening. At synchrotron sources, native crystals diffracted to 2.9 Å, and selenomethionine-substituted crystals diffracted to 3.3 Å. Both native and selenomethionine crystals belonged to space group $P4_1$ (native unit cell dimensions, a = 107.9 Å, b = 107.9 Å, c = 46.1 Å, $\alpha = \beta = \gamma = 90°$; Se–Met unit cell dimensions, a = 108.2 Å, b = 108.2 Å, c = 46.6 Å, $\alpha = \beta = \gamma = 90°$) and contained approximately 70% solvent. Initial phases for Sec17 were obtained from anomalous diffraction of selenomethionine-substituted crystals and were improved using solvent flipping (Abrahams and Leslie, 1996), histogram matching (Zhang and Main, 1990), and phase extension with the native data (Table 1). Electron density maps obtained from these initial phases and native amplitudes clearly revealed all 14 α helices (Figure 1) and most of the connecting loops and were readily traced. Density-modified experimental phases were used

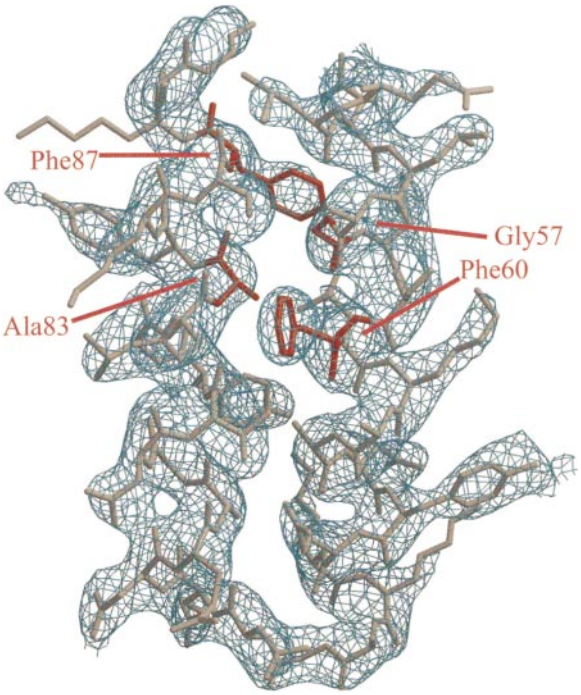

Figure 1. Experimental Electron Density Map after Density Modification

Density-modified experimental electron density for α helices α3 and α4 and the connecting loop contoured at 1.4 σ. The final, refined model is shown using a ball-and-stick representation. The α helices, loop, and most side chains are clearly visible in the initial map. The buried residues Gly-57, Phe-60, Ala-83, and Phe-87, which are conserved in the representative SNAP sequences (Figure 3a), are depicted in red.

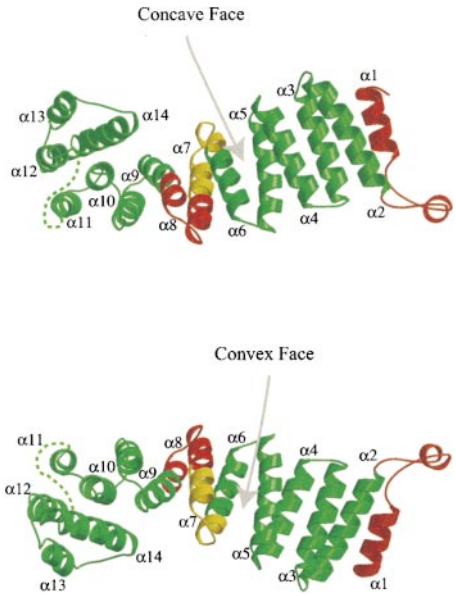

Figure 2. Overall Structure of Sec17

Two ribbon drawings of Sec17 related by a 180° rotation around the long axis of the protein. The nine N-terminal α helices form a twisted sheet that gives rise to two faces and two ridges. The five C-terminal α helices form a more globular bundle, which is asymmetrically disposed with respect to the N-terminal sheet, creating a significant cleft on one face of the molecule. Residues colored red and yellow correspond, respectively, to inhibitory and noninhibitory peptides from an earlier study (DeBello et al., 1995).

throughout the refinement process in order to minimize model bias and ensure the most accurate model possible (Pannu et al., 1998). The free R value (Brunger, 1992) for the final model is 28.3% for all reflections in the test set with Bragg spacings between 500 and 2.9 Å.

General Features of the Structure

The 14 α helices of Sec17 assemble into a relatively extended, asymmetric structure (Figure 2). The dimensions of the protein are approximately 85 Å × 35 Å × 35 Å. The solvent-exposed surface area of Sec17 is 15,000 Å^2, which is greater than that expected for a typical globular monomeric protein of this size (approximately 12,000 Å^2) (Miller et al., 1987). The N-terminal region consists of a twisted sheet of nine α helices, each containing roughly 14 residues. With the exception of α helices α1 and α2, which are connected by an extended loop (Figure 2), the other α helices in the N-terminal domain are connected by short loops of 2–5 residues. Eight of these α helices form tandemly repeated antiparallel pairs (α2–α3, α4–α5, α6–α7, and α8–α9). These hairpin repeats are structurally very similar to one another: pairwise superposition gives C_α rmsds ranging from 0.65 Å (for α2–α3 and α4–α5) to 1.28 Å (for α2–α3 and α8–α9). Within each repeat, the α-helical crossing angle is around 24°. The first two repeats are related by a 24° rotation, while subsequent pairs are related by a 30° rotation. Due to the packing between adjacent repeats in the N-terminal sheet of α helices, a significant right-handed twist accumulates, and the first α helix of the sheet is roughly perpendicular to the last (Figure 2). The C-terminal region contains a globular bundle formed by five α helices of variable length connected by loops of variable length. This α-helical bundle is asymmetrically disposed with respect to the plane of the extended N-terminal domain (Figure 2). The combination of the sheet-like N-terminal domain and the protruding C-terminal bundle results in two faces of very different character: one convex, the other concave and presenting a cleft formed by the intersection of the two domains (Figure 2).

Conserved Residues: Packing and Surface Features

Many of the strongly conserved residues are located in the packing interface between α helices (Figure 3a). These residues are the principal determinants of the relative orientation between neighboring α helices, and, consequently, of the overall twist of the sheet of α helices. The sequence conservation of these packing residues suggests that SNAP proteins have a conserved three-dimensional shape. For example, Gly-57 is conserved in the six representative SNAP sequences examined (Figure 3a). This residue contacts other conserved residues, Phe-60 on the same α helix and Ala-83 and Tyr-87 on the adjacent α helix (Figure 1), and thus permits a close packing interaction between α helices α3 and α4 (Figure 1).

Not all the conserved residues are involved in α helix packing (Figures 3a and 4a). Several conserved residues are solvent exposed, and some of them participate in

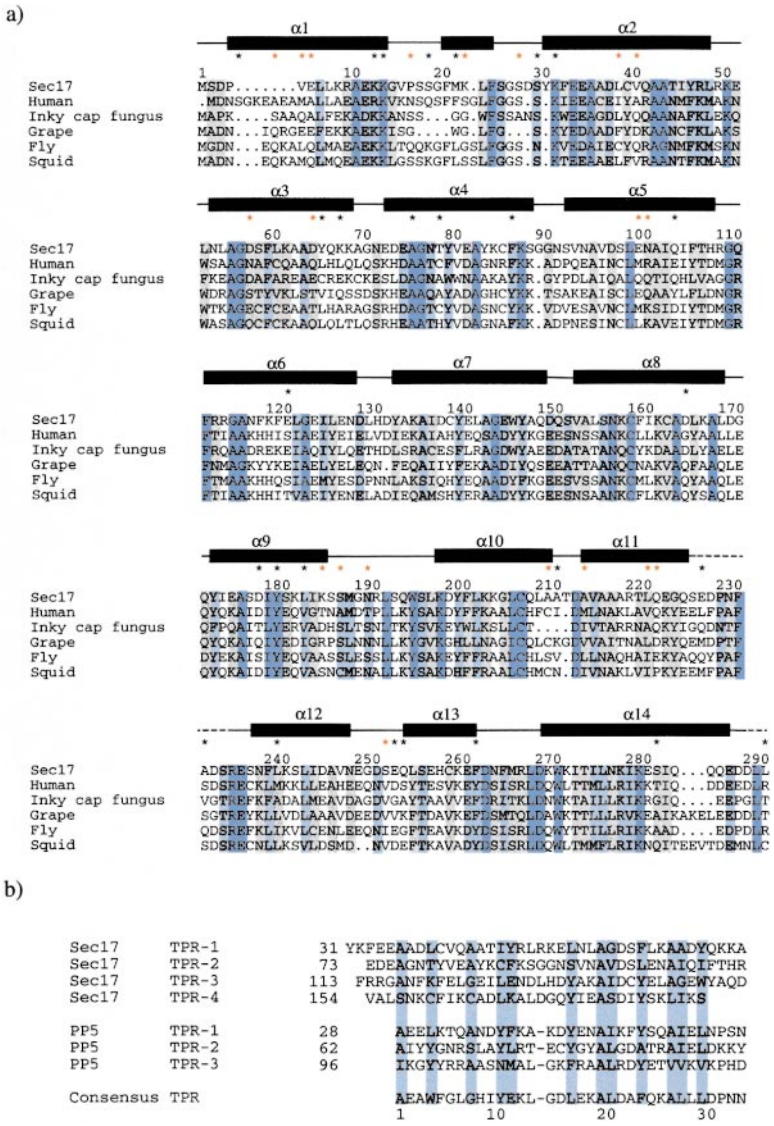

b)

Figure 3. Conserved Features of the Sequence

(a) Six representative SNAP sequences (*Saccharomyces cerevisiae*, *Homo sapiens*, *Coprinum cinereus*, *Vitis vinifera*, *Drosophila melanogaster*, and *Oligo pealei*) were aligned using ClustalW (Thompson et al., 1994). The multiple sequence alignment was analyzed using AMAS (Livingstone and Barton, 1993) with the intra_cl matrix. Absolutely conserved positions (AMAS score greater than 10) are highlighted with dark blue boxes, strongly conserved positions (AMAS score 8 or 9) with light blue boxes, and weakly conserved positions (AMAS score 6 or 7) with gray boxes. α-helical regions are indicated above the alignment by solid boxes, and loops are indicated by a solid line. The loop between α11 and α12 and the two residues at the C terminus are disordered in the crystal structure and were therefore not traced. These missing residues are indicated by dashed lines. An asterisk above the sequence alignment indicates a position where the sequences of bovine α-SNAP and β-SNAP differ. Conservative differences are shaded black, and nonconservative changes red.

(b) Multiple sequence alignment of the four TPR-like repeats of Sec17, the three TPRs of PP5 (Das et al., 1998), and a consensus TPR (Sikorski et al., 1990). The consensus TPR sequence was taken from a number of proteins not including PP5. Blue shading indicates consensus TPR motif residues identified in the structure of the TPRs from PP5 (Das et al., 1998).

polar interactions that may be important in determining the overall shape of the protein. For example, the absolutely conserved residue Lys-14 forms a salt bridge with the strongly conserved Glu-35, an interaction likely to be important in determining the interaction between the first and second α helices, and in stabilizing the end points of the intervening, extended loop.

Projecting the degree of sequence conservation onto the surface of Sec17 reveals characteristic features. There is an alternating pattern of loop conservation thoughout most of the sequence wherein every other loop shows significant conservation (loops α5–α6, α7–α8, α9–α10, α11–α12, and α13–α14) (Figure 3a). Most residues in these loops are solvent exposed and do not participate in specific intramolecular interactions. The pattern of sequence conservation makes it such that one edge of the sheet of α helices (Figures 2, top, and 4a, left panel) is more conserved than the other (Figures 2, bottom, and 4a, right panel). There is also a marked difference in the sequence conservation between the two faces of the protein: the concave face (Figures 2, top, and 4a, left panel) shows a higher degree of conservation than the convex one (Figures 2, bottom, and 4a, right panel).

There is also a striking difference in the electrostatic surface potential of the convex and concave faces of Sec17 (Figure 4b). The convex face has a negative charge distribution, which is most pronounced at the extreme C terminus. The concave face is characterized by a slightly basic, mottled charge distribution.

β-SNAP is a neuronal isoform of α-SNAP that has been suggested to have different biochemical properties (Schiavo et al., 1995; Colombo et al., 1998). Differences in the sequences of α- and β-SNAP are concentrated in two regions (Figure 3a): an N-terminal region encompassing α1 to α5, and a C-terminal region encompassing α9 to α11. This emphasizes the variable nature of the extreme N terminus of SNAPs. It also suggests that the N-terminal portion of the sheet of α helices and the junction between the sheet and the C-terminal bundle may be important sites of interaction with other SNAP effectors.

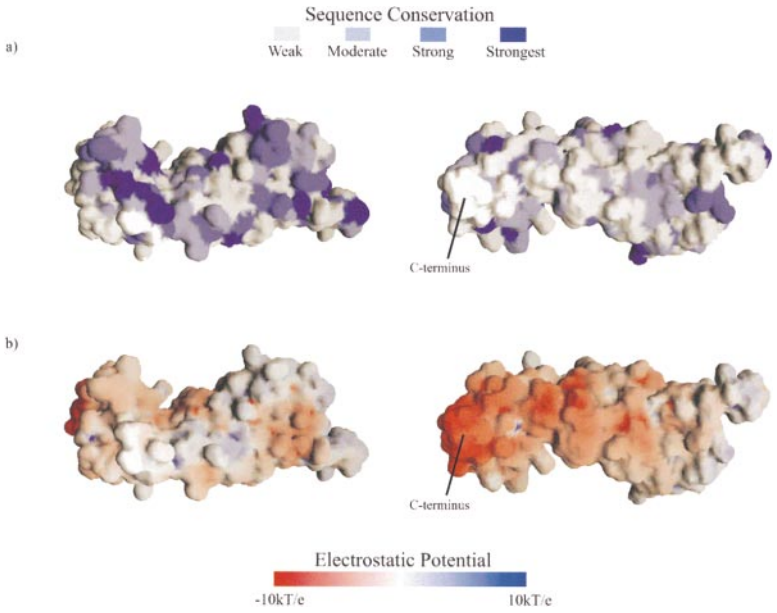

Figure 4. Surface Features of Sec17

(a) Sequence conservation projected onto the accessible surface of Sec17. The degree of sequence conservation was projected onto the solvent-accessible surface as calculated by GRASP (Nicholls et al., 1991). Variable regions are colored in white, and increasing conservation is indicated with increasingly dark blue. Two views of the protein are shown. The flatter, convex face (right panel, same view as Figure 2, bottom) is significantly less conserved that the concave one (left panel, same view as Figure 2, top).

(b) Electrostatic surface potential. Two views of the electrostatic surface potential of Sec17 are shown. The two views are identical to those in Figures 2 and 4a. Hydrogens were generated using CNS (Brunger et al., 1998), and the electrostatic surface potential was computed with GRASP (Nicholls et al., 1991) using the OPLS parameters (Jorgensen and Tirado-Rives, 1988). The electrostatic potential is contoured at the 10 kT/e level, with red denoting negative potential and blue, positive potential. Note the strong negative character of the C-terminal region, the largely negative character of the convex face (right panel), and the basic character of the more conserved, concave face (left panel).

Comparison to Tetratricopeptide Repeats

Three-dimensional alignment using DALI (Holm and Sander, 1993) of the Sec17 structure against a representative set of structures in the PDB reveals that regions of Sec17 share significant structural similarity with several previously determined protein folds (see below), most notably with the structure of the tetratricopeptide repeats (TPRs) in the regulatory domain of protein phosphatase 5 (PP5) (Das et al., 1998). TPRs are degenerate 34–amino acid sequence motifs present in a wide variety of proteins, many of which participate in protein–protein interactions in processes as diverse as mitosis, RNA synthesis, and chaperone function (Sikorski et al., 1990; Lamb et al., 1995). TPRs do not have any absolutely conserved residues; instead, they are characterized by a conserved pattern of small and large hydrophobic residues (Sikorski et al., 1990; Lamb et al., 1995). A single TPR repeat folds into an antiparallel helix-loop-helix structure that is largely determined by knob-into-hole packing of the consensus large and small residues (Das et al., 1998).

Comparative sequence analysis of proteins from widely different organisms has identified at least 25 different proteins that contain TPRs (Lamb et al., 1995). Sequence analysis also indicated that similar domains would be present in the SNAP family (Ordway et al., 1994). The TPR-like sequences in Sec17 differ from the consensus TPR sequence in several key ways (Figure 3b). The TPR-like sequences in Sec17 have an insertion of one amino acid in the loop between α helices. They also lack the consensus proline at position 32 and have a smaller than average residue at position 21. Nevertheless, pairwise superposition of the four antiparallel α-helical repeats of Sec17 to the three TPRs of PP5 shows structural conservation, with C_α rmsd values ranging from 0.37 Å to 1.51 Å.

Despite the local structural similarity of the Sec17 repeats to TPRs, the overall twist of the sheet of α helices in Sec17 differs significantly from that of PP5 (Figure 5). Sec17 forms a much flatter structure than do the TPRs from PP5, and, accordingly, the superhelical pitch of Sec17 is double that of the TPRs from PP5 (Das et al., 1998). This large difference between two proteins built from very similar α-helical hairpin units has implications for all TPR-containing proteins. The more pronounced curvature of the TPRs in PP5 forms a groove that binds to a peptide in an extended conformation (Das et al., 1998). The width and depth of this groove depend directly on the twist of the sheet of α helices, and in the structure of Sec17 the groove is much broader and shallower (Figure 5). This variability in the groove shape may have implications for the binding activity of TPR-containing proteins: in contrast to the TPRs from PP5, a shallow groove such as that seen in Sec17 is poorly suited to bind a peptide in extended conformation. TPR-containing proteins may therefore bind a wider variety of substrates using a wider variety of binding modes than previously suggested (Das et al., 1998).

Comparison to Other α/α Proteins

Sec17 also shows superficial local similarity to several other proteins composed of α-helical repeats (Figure 5), including HEAT repeats (Chook and Blobel, 1999; Cingolani et al., 1999; Groves et al., 1999; Vetter et al., 1999), armadillo repeats (Huber et al., 1997; Conti et al., 1998), and clathrin heavy chain repeats (Ybe et al., 1999) (Figure 5). All of these proteins mediate protein–protein interactions, an activity that is relevant to the function of SNAPs in intracellular membrane fusion. In spite of significant differences between all these proteins, they share common structural features related to their binding activity. The superhelical arrangement of repeats

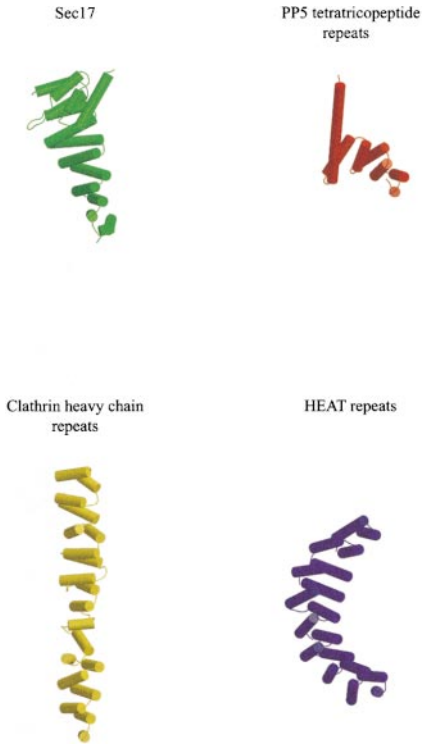

Figure 5. Comparison of Several α-Helical Repeat Motifs

Comparative cartoon representations of four different proteins composed of α-helical repeats: Sec17 residues 1–290 (green), tetratricopeptide repeats from PP5 residues 19–165 (red), clathrin heavy chain repeat residues 1210–1516 (yellow), and the HEAT repeats from the PR65/A subunit of PP2A residues 120–474 (purple). All proteins are shown with the first α helix of the first repeat approximately perpendicular to the plane of the figure in order to emphasize the different curvatures of the sheets of α helices. In addition to well-defined ridges, all four proteins have two primary surfaces of distinct character, one concave and one convex.

generally gives rise to two distinct "faces", one concave and the other convex (Figures 2 and 5). In some of these proteins, notably the TPRs from PP5 (Das et al., 1998) and the armadillo repeats from karyopherin-α (Conti et al., 1998), and the HEAT repeats in importin-β (also called karyopherin-β) (Cingolani et al., 1999), this concave surface was shown to constitute the binding surface for interactions with target proteins. The flat nature of the clathrin heavy chain repeat surface (Ybe et al., 1999) results in two fairly similar faces that were postulated to form a scaffold for protein–protein interactions. The structure of the HEAT repeats from the PR65/A subunit of PP2A (Groves et al., 1999) was determined in the absence of any interacting substrate, but based upon a variety of biochemical data, a ridge formed by loops in the repeating unit was proposed to constitute the main interaction interface.

Interactions with SNAREs

Deletion mutagenesis and in vitro binding assays suggested that some of the first 63 and some of the last 37 residues of α-SNAP are essential for binding to the SNARE complex (Hayashi et al., 1995). Interestingly, deletion of the 28 N-terminal residues reduced α-SNAP binding to the ternary SNARE complex by 75% but did not affect binding to NSF or activation of NSF's ATPase activity (Hayashi et al., 1995). Given that the first 17 residues of Sec17 are not required for its function in vivo (Griff et al., 1992) and that the first 30 residues in the structure form a single α helix and long loop with a single α-helical turn (Figure 2), it is likely that the first 28 residues are not required for proper folding of the entire protein. These observations imply that some of these N-terminal residues interact with the SNARE complex or participate in SNAP:SNAP interactions that are important for SNARE binding. It is difficult to make a similar statement regarding the C-terminal 37 residues since they include helices α13 and α14 and are probably required for the proper folding of the entire protein. Indeed, residues of helix α14 interact with residues in five of the other α helices of Sec17. Thus, the available biochemical data (Griff et al., 1992; Hanson et al., 1995; Hayashi et al., 1995; Barnard et al., 1996) suggest that at least some residues important for SNARE binding reside near the N terminus of SNAPs. EM images of SNAP:SNARE complexes (Hohl et al., 1998) indicated that SNAPs covered the SNARE complex in a sheath-like manner, and so it is likely that SNARE-contacting residues are distributed throughout a large part of the SNAP sequence.

Injection of SNAP or SNAP-related peptides into the giant synapse of squid has been used to characterize SNAP function in neurotransmitter release (DeBello et al., 1995). Injection of full-length SNAP enhanced neurotransmitter release. Injection of a peptide corresponding to residues 127–144 of mammalian α-SNAP (equivalent to 125–142 of Sec17) had no effect on neurotransmitter release, but injection of peptides corresponding to residues 1–24 and 19–31 of squid SNAP (equivalent to 1–21 and 19–31 of Sec17) and 144–163 of mammalian α-SNAP (equivalent to 140–159 of Sec17) all had a significant inhibitory effect. These peptides presumably exerted their inhibitory effect by competitively interfering with SNAP:SNARE binding or with SNAP:NSF binding. The crystal structure of Sec17 reveals that the injected peptides contain loop sequences (Figure 2). This was not anticipated in the original study, which was carried out without knowledge of the SNAP crystal structure. It is striking that the inhibitory peptides and noninhibitory peptides map to opposing ridges of Sec17 (Figure 2), with inhibitory peptides located on the more conserved ridge (Figures 2, top, and 4a, left panel).

Based on sequence analysis, biochemical data, and electron microscopic images of SNAP:SNARE and of NSF:SNAP:SNARE complexes (Hanson et al., 1997; Hohl et al., 1998), one can speculate about possible modes of association between SNAPs, SNAREs, and NSF/Sec18. SNAPs are relatively promiscuous in their ability to bind SNARE complexes. The large sequence variation between SNAREs of a given species, especially on the surface of the four-helix bundle (Fasshauer et al., 1998b), makes it likely that SNAPs primarily recognize the overall shape of the four-helix bundle SNARE complex instead of choosing a number of sequence-specific contacts. Images of the SNAP:SNARE complex showed that SNAP bound in a lateral fashion along the length of the SNARE bundle (Hohl et al., 1998). Furthermore, antibody-decorated images of the 20S SNAP:SNARE:NSF complex showed that the N terminus of SNAP was localized near the C-terminal membrane anchors of the SNARE complex (Hohl et al., 1998).

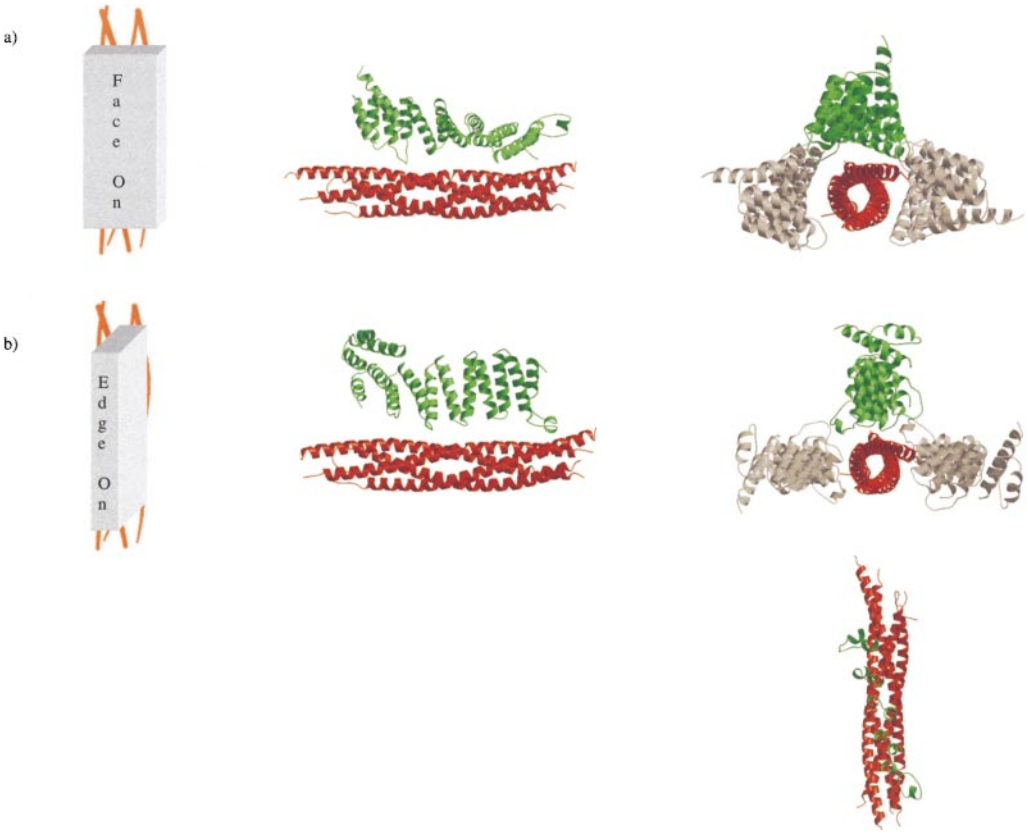

Figure 6. Models of SNAP:SNARE Interaction

(a) Face-on longitudinal interaction. In the left panel, the SNARE complex is represented in red by the local helical axes of each of the four α helices of the core synaptic fusion complex (Sutton et al., 1998). The SNAP is represented by a three-dimensional rectangular solid. Face-on interaction occurs when the broad surface of SNAP contacts the SNARE bundle, and longitudinal interaction occurs when the long axis of SNAP is coincident with the long axis of the SNARE complex. In the middle and right panels are cartoon representations of face-on longitudinal SNAP:SNARE interactions. A single Sec17 molecule was modeled onto the SNARE complex (middle panel), and two additional copies were generated by ±90° rotations around the central axis of the bundle (right panel).

(b) Edge-on longitudinal interaction. Again, in the left panel, the SNARE complex is represented in red by the local helical axes of each of the four α helices of the core synaptic fusion complex (Sutton et al., 1998). The SNAP is represented by a three-dimensional rectangular solid. Edge-on interaction occurs when the ridge of SNAP contacts the SNARE bundle. In the middle and right panels are cartoon representations of edge-on longitudinal SNAP:SNARE interactions. A single Sec17 molecule was modeled onto the SNARE complex (middle panel), and two additional copies were generated by ±90° rotations around the central axis of the bundle (right panel). In the bottom right panel is a cartoon drawing illustrating the shape complementarity in the edge-on interaction. For clarity, only the loops and four residues from each α helix of Sec17 are shown.

By analogy with the α/α proteins discussed above, one can imagine four general configurations for a SNAP:SNARE complex, two longitudinal modes wherein the long axis of SNAP is roughly coincident with the long axis of the SNARE complex, and two transverse modes wherein the long axis of the SNAP is roughly orthogonal to the long axis of the SNARE complex. There are two extreme longitudinal or transverse modes: "face-on" and "edge-on" (Figure 6). In constructing face-on or edge-on models of SNAP:SNARE interaction, we restricted our attention to the face and ridge showing higher sequence conservation for three reasons (Figures 2 and 4a). First, this conserved ridge contains most of the sequences present in the inhibitory peptides used in a previous study (DeBello et al., 1995). Second, for the conserved face, this assumption is also consistent with the binding modes of other α/α proteins that use the concave face as a binding surface. Third, it is more consistent with electrostatic considerations because it matches the more basic surface of Sec17 to the largely negative charge distribution at the surface of the SNARE complex (Sutton et al., 1998).

Transverse modes of association are unlikely for a number of reasons. For a transverse, face-on interaction (data not shown), the length of the intermolecular interface would be limited to around 35 Å (the width of Sec17), and based on deletion mutagenesis, it seems likely that SNAP contacts a larger region of the SNARE complex (Hanson et al., 1995; Hayashi et al., 1995; Kee et al., 1995). Furthermore, the electron microscopic images of SNAP:SNARE complexes (Hohl et al., 1998) showed a widening along the entire length of the SNARE bundle, which suggests a longitudinal association. Finally, a transverse binding mode would not explain the inhibitory effect of injected peptides (DeBello et al., 1995) because at least one of the corresponding loops would be distant from both the SNARE complex and NSF/Sec18.

In longitudinal face-on mode (Figure 6a), the conserved face of SNAP would interact lengthwise with the SNARE complex. This mode of association would result in approximately perpendicular α helix packing between SNAP and SNAREs. In longitudinal edge-on mode (Figure 6b), the conserved ridge of SNAP would interact lengthwise with the SNARE complex, most likely with one of the surface grooves. In this type of interaction, loops between the α helices of SNAP would provide a large part of the interface, and it is striking that the curvature defined by the conserved ridge is complementary to that of a surface groove of the SNARE complex (Figure 6b).

The lack of specific biochemical data makes it difficult to distinguish between the two longitudinal modes. The interactions between SNAPs, SNAREs, and NSF/Sec18 have to reconcile two mutually incompatible symmetries: the approximately four-fold symmetry of the SNARE complex and the six-fold symmetry of NSF/Sec18. It has been estimated that three SNAP molecules (Hayashi et al., 1995; Rossi et al., 1997) bind to one SNARE complex and that this SNAP:SNARE complex then binds to a single NSF/Sec18 hexamer. Thus, for both face-on and edge-on longitudinal binding, three models of Sec17 were placed along the SNARE complex such that each SNAP recognizes similar features of the SNARE complex, such as a surface groove (Figure 6).

Interactions with Sec18 (NSF)

The face-on and edge-on longitudinal models of SNAP:SNARE binding have features in common that may be relevant to the function of SNAPs in the disassembly of SNARE complexes. Sequence conservation, electrostatic considerations, and the peptide injection study (DeBello et al., 1995) were used to identify one face (concave, Figure 2, top panel) and one ridge (Figure 2, top panel, bottom edge) of the structure as probable SNARE or NSF/Sec18 interaction surfaces. In both the face-on and edge-on models consistent with this assumption, the C-terminal bundle of Sec17 protrudes from the long axis of the SNAP/SNARE complex (Figure 6). The penultimate residue of α-SNAP (a conserved leucine, Figure 3a) is critical for stimulation of the ATPase activity of NSF (Barnard et al., 1997), and in both the face-on and edge-on longitudinal models, this residue is located most distal to the center of the SNARE bundle (Figure 6), accessible for interacting with NSF/Sec18.

Along with some striking similarities, there is a key difference between the face-on and the edge-on model. The face-on model allows for SNAP:SNAP contacts, which occlude a large fraction of the SNARE complex's surface at the same time that they bury most of the conserved surfaces of the SNAP. The face-on model of SNAP:SNARE binding may preclude binding of other factors (such as synaptotagmin [Brose et al., 1992; Schiavo et al., 1995] for the neuronal SNAREs, or a Sec1 family member [reviewed in Halachmi and Lev, 1996]). The edge-on model shows shape complementarity between a surface groove of the SNARE bundle and the conserved ridge of SNAPs (Figure 6b). It also leaves a large portion of both the SNARE bundle and the conserved SNAP surfaces exposed to solvent. The face-on and edge-on models are therefore very different in the types of interactions they allow with other SNARE-binding proteins. We present both models as probable extremes, and it is likely that the true mode of SNAP:SNARE interaction lies somewhere between the two. It is also possible that multiple SNAP:SNARE binding modes exist.

Electron microscopic images of NSF bound to various adenosine nucleotides or analogs suggest that NSF/Sec18 undergoes significant conformational changes in the form of domain motions upon ATP hydrolysis by the D1 domain (Hanson et al., 1997). The recently determined structure of the N-terminal SNARE-binding domain of NSF (Yu et al., 1999) shows significant similarity to a domain in EF-Tu, a well-characterized protein that also uses nucleotide hydrolysis to produce a large conformational change in the form of domain rearrangements (Kjeldgaard et al., 1993). In the simplest terms, large-scale motion of the N-terminal domain of NSF could be used to generate a mechanical force acting on the SNARE complex. The relatively flat structure of Sec17 with its faces and ridges seems well suited to the transmission of force. It is likely that there is a direct interaction between NSF and the conserved, penultimate leucine. The fact that our models of SNAP:SNARE binding place this residue most distal from the center of the SNARE bundle raises the possibility that SNAPs function as lever arms, transmitting forces generated by domain rearrangments in NSF upon ATP hydrolysis.

Figure Preparation

Figures were prepared using Molscript (Kraulis, 1996), Bobscript (Esnouf, 1997), GRASP (Nicholls et al., 1991), Raster3D (Merritt and Bacon, 1997), and GL_RENDER (courtesy of Lothar Esser).

Experimental Procedures

Cloning and Expression

Sec17 was expressed as previously described (Rossi et al., 1997) using the GST fusion expression vector pGEX-4T-1 (Pharmacia), which produces a thrombin-cleavable fusion between Sec17 and glutathione S-transferase. Nucleotide sequencing of the Sec17 cDNA insert indicated the presence of a single point mutation, which substituted an isoleucine for the N-terminal methionine. The plasmid was introduced into BL21 cells and grown in terrific broth supplemented with 0.1 mg/ml ampicillin. Cells were grown at 37°C to an optical density of A_{600} ~1, shifted to 30°C for about 45 min, and induced with 0.8 mM IPTG for 3–4 hr. Cells were harvested by centrifugation and stored at −80°C. For protein purification, typically 35 g of cells were resuspended in 150 ml of 20 mM Tris (pH 8.0), 250 mM NaCl, 5 mM EDTA, 10 mM DTT, and 1 mM PMSF and homogenized by sonication. The cell lysate was centrifuged for 30 min at 26,000 × g, and the supernatant was incubated with 10 ml glutathione Sepharose 4B (Pharmacia) for 45 min at 4°C. After binding, the resin was washed twice with lysis buffer and twice with thrombin buffer (20 mM Tris [pH 8.0], 50 mM NaCl, 10 mM DTT). The resin was resuspended in an equal volume of thrombin buffer and incubated with about 50 μg of bovine thrombin (Haematologic Technologies) overnight at 4°C. After cleavage, the Sec17-containing supernatant was loaded on a 16/10 Mono-Q column (Pharmacia) and eluted with a linear gradient of NaCl from 200 to 500 mM. Purified protein was dialyzed against protein buffer (20 mM Tris [pH 8.0], 100 mM NaCl, 10 mM DTT), concentrated to 25 mg/ml, flash frozen in liquid nitrogen, and stored at −80°C. Se–Met protein was produced as above, except for the following: B834(DE3) (Novagen) cells were used for expression and were grown in Se–Met

containing defined media (Leahy et al., 1994). Se–Met protein was concentrated to 12.5 mg/ml for storage and crystallization.

Crystallization, Data Collection, and Processing

Crystals were originally grown using hanging drop vapor diffusion at 4°C. Three to four microliters of 25 mg/ml native protein was mixed with 1 μl of mother liquor consisting of 100 mM sodium citrate (pH 5.9), 200 mM NaCl, 1.5%–2% polyethyleneimine, 3% glycerol, and 10 mM DTT on a siliconized glass coverslip and equilibrated against 0.5 ml of mother liquor. Crystals grew to full size (about 0.5 mm × 0.05 mm × 0.05 mm) within 24 hr. Crystals appeared stable under these conditions but were in fact slowly deteriorating as determined by diffraction images. This was ascribed to continuing equilibration of the protein/mother liquor mixture and was compensated for by growing crystals using microbatch techniques. As with the vapor diffusion trials, native protein was mixed with mother liquor (containing between 200 and 500 mM NaCl) at ratios between 3:1 and 4:1 in a total volume of 15 μl. These mixtures were equilibrated at room temperature for 30 min and then centrifuged for 20 s in a benchtop microfuge at maximum speed before sealing the supernatant in a 25 μl container (micro bridges, Hampton Research) at 4°C. This resulted in improved, stable crystals, and hence, all data collection was performed on crystals grown in batch. Selenomethionine-labeled protein grew under similar conditions with the exception that the protein and polyethyleneimine concentrations were lower, 12.5 mg/ml and 1%, respectively. Native crystals were serially soaked for about 10 s per solution in stabilization solutions containing 6, 12, 18, 24, and 30% glycerol (in addition to the condition of the batch trials) before flash freezing in liquid nitrogen–cooled propane. Selenomethionine crystals were frozen in a similar manner with the exception that the concentration of polyethyleneimine was linearly decreased to 0% in the final solution. Sec17 crystallized in space group $P4_1$ with one molecule per asymmetric unit and about 70% solvent. Anomalous diffraction data at two wavelengths were collected at 100 K at beamline 5.02 at the Advanced Light Source (ALS) using a Quantum-4 CCD detector (Area Detector Systems Corporation) (Table 1). Anomalous data corresponding to the peak anomalous signal and first inflection point were collected in 15° wedges using inverse beam geometry. A complete diffraction data set was collected at the first wavelength before moving on to the second. Presumably due to radiation damage and an intrinsically weak signal, the dispersive differences between the two wavelengths were unacceptably high and therefore not used for MAD phasing (Table 1). Native diffraction data (Table 1) were collected at the same beamline. Data were processed using DENZO (Otwinowski and Minor, 1997), and intensities were reduced and scaled using SCALEPACK (Otwinowski and Minor, 1997) (Table 1).

Structure Determination

All calculations after data processing were performed using the Crystallography and NMR System (CNS) (Brunger et al., 1998). The three expected selenium sites were found using an automated Patterson heavy-atom search method (Grosse-Kunstleve and Brunger, 1999) using data from the peak anomalous wavelength. Due to the problems with the dispersive differences, SAD phasing was performed separately for both wavelengths. Phase probability distributions for each wavelength were then combined prior to density modification and phase extension using the native data. Heavy atom parameter refinement was carried out using a maximum likelihood target function (Burling et al., 1996), with atomic f′ and f′′ values constrained to be equal for all three sites. Forty cycles of solvent flipping (Abrahams and Leslie, 1996) and histogram matching (Zhang and Main, 1990) were performed for the density modification.

Model Building and Refinement

The initial model was built using the program O (Jones et al., 1991). Fourteen idealized 15-residue polyalanine α helices were manually placed into the initial electron density map obtained by SAD phasing, phase combination, density modification, and phase extension. A region of this map is depicted in Figure 1. There is clear electron density for the two α helices, the connecting loop, and most side chains. Nearly all the loops connecting α helices were visible in the initial map, and in conjunction with the three selenium sites, it was relatively straightforward to trace the loops and assign the entire sequence of the protein. The progress of model refinement was monitored using the free R value (Brunger, 1992) computed from a randomly omitted 10% of the observed diffraction data. Refinement consisted of alternating rounds of torsion angle molecular dynamics simulated annealing (Rice and Brunger, 1994), restrained atomic B factor refinement (Hendrickson, 1985), and model rebuilding in O (Jones et al., 1991). All model refinement employed the MLHL target function (Pannu et al., 1998) with the density-modified phases used as a prior phase probability distribution. Refinement was carried out against the native diffraction amplitudes and used a flat bulk solvent correction (Jiang and Brunger, 1994) (electron density level $\rho_{sol} = 0.345$ e/Å^3, $B_{sol} = 31.7$ Å^2) and overall anisotropic B factor correction ($B_{11} = 7.259$ Å^2, $B_{22} = 7.259$ Å^2, $B_{33} = -14.517$ Å^2, $B_{12} = B_{13} = B_{23} = 0$ Å^2) at 500–2.9 Å resolution. The final model consists of residues 1–227, 237–290, and four water molecules. Final model statistics are shown in Table 1.

Acknowledgments

We thank Chris Stroupe and Rich Yu for assistance with data collection, and Craig Ogata (Brookhaven X4A), Marian Sbzenyi (CHESS F2 and A1), Thomas Earnest, and Li-Wei Hung (ALS 5.02) for advice at various beamlines (ALS is funded by the US Department of Energy Office of Basic Energy Sciences). We are grateful to Christian Ostermeier for advice concerning crystallization, to Paul D. Adams for advice concerning model building and refinement, and to Lothar Esser for access to the program GL_RENDER. We also thank Reinhard Jahn for stimulating discussions, Peter Hwang for providing the clathrin coordinates prior to publication, and Rich Yu, Satwik Kamtekar, Paul Adams, Bryan Sutton, and Mark Bowen for a critical reading of the manuscript. L. M. R. is an HHMI predoctoral fellow.

Received April 29, 1999; revised June 7, 1999.

References

Abrahams, J.P., and Leslie, A.G.W. (1996). Methods used in the structure determination of bovine mitochondrial F1 ATPase. Acta Crystallogr. D *52*, 30–42.

Barnard, R.J.O., Morgan, A., and Burgoyne, R.D. (1996). Domains of α-SNAP required for the stimulation of exocytosis and for N-ethylmaleimide-sensitive fusion protein (NSF) binding and activation. Mol. Biol. Cell *7*, 693–701.

Barnard, R.J.O., Morgan, A., and Burgoyne, R.D. (1997). Stimulation of NSF ATPase activity by α-SNAP is required for SNARE complex disassembly and exocytosis. J. Cell Biol. *139*, 875–883.

Brose, N., Petrenko, A.G., Südhof, T.C., and Jahn, R. (1992). Synaptotagmin: a calcium sensor on the synaptic vesicle surface. Science *256*, 1021–1025.

Burling, F.T., Weis, W.I., Flaherty, K.M., and Brunger, A.T. (1996). Direct observation of protein solvation and discrete disorder with experimental crystallographic phases. Science *271*, 72–77.

Brunger, A.T. (1992). Free R value: a novel statistical quantity for assessing the accuracy of crystal structures. Nature *355*, 472–475.

Brunger, A.T., Adams, P.D., Clore, G.M., DeLano, W.L., Gros, P., Crosse-Kunstleve, R.W., Jiang, J.S., Kusewski, J., Nilges, M., Pannu, N.S., et al. (1998). Crystallography and NMR system (CNS): a new software system for macromolecular structure determination. Acta Crystallogr. D *54*, 905–921.

Chen, Y.A., Scales, S.J., Patel, S.M., Doung, Y.-C., and Scheller, R.H. (1999). SNARE complex formation is triggered by Ca^{2+} and drives membrane fusion. Cell *97*, 165–174.

Chook, Y.M., and Blobel, G. (1999). Structure of the nuclear transport complex karyopherin-β2-Ran·GppNHp. Nature *399*, 230–237.

Cingolani, G., Petosa, C., Weis, K., and Müller, C.W. (1999). Structure of importin-β bound to the IBB domain of importin-α. Nature *399*, 221–229.

Clary, D.O., Griff, I.C., and Rothman, J.E. (1990). SNAPs, a family of NSF attachment proteins involved in intracellular membrane fusion in animals and yeast. Cell *61*, 709–721.

Colombo, M.I., Gelberman, S.C., Whiteheart, S.W., and Stahl, P.D. (1998). N-ethylmaleimide-sensitive factor-dependent α-SNAP release, an early event in the docking/fusion process, is not regulated by Rab GTPases. J. Biol. Chem. *273*, 1334–1338.

Conti, E., Uy, M., Leighton, L., Blobel, G., and Kuriyan, J. (1998). Crystallographic analysis of the recognition of a nuclear localization signal by the nuclear import factor karyopherin α. Cell *94*, 193–204.

Das, A.K., Cohen, P.T.W., and Barford, D. (1998). The structure of the tetratricopeptide repeats of protein phosphatase 5: implications for TPR-mediated protein-protein interactions. EMBO J. *17*, 1192–1199.

DeBello, W.M., O'Connor, V., Dresbach, T., Whiteheart, S.W., Wang, S.S.-H., Schweizer, F.E., Betz, H., Rothman, J.E., and Augustine, G.J. (1995). SNAP-mediated protein-protein interactions essential for neurotransmitter release. Nature *373*, 626–630.

Eakle, K.A., Bernstein, M., and Emr, S.D. (1988). Characterization of a component of the yeast secretion machinery: identification of the sec18 gene product. Mol. Cell. Biol. *8*, 4098–4109.

Esnouf, R.M. (1997). An extensively modified version of MOLSCRIPT that includes greatly enhanced coloring capabilities. J. Mol. Graph. Model *15*, 132–134.

Fasshauer, D., Eliason, W.K., Brunger, A.T., and Jahn, R. (1998a). Identification of a minimal core of the synaptic SNARE complex sufficient for reversible assembly and disassembly. Biochemistry *37*, 10354–10362.

Fasshauer, D., Sutton, R.B., Brunger, A.T., and Jahn, R. (1998b). Conserved structural features of the synaptic fusion complex: SNARE proteins reclassified as Q- and R-SNAREs. Proc. Natl. Acad. Sci. USA *95*, 15781–15786.

Ferro-Novick, S., and Jahn, R. (1994). Vesicle fusion from yeast to man. Nature *370*, 191–193.

Fiebig, K.M., Rice, L.M., Pollock, E., and Brunger, A.T. (1999). Folding intermediates of SNARE complex assembly. Nat. Struct. Biol. *6*, 117–123.

Graham, T.R., and Emr, S.D. (1991). Compartmental organization of golgi-specific protein modification and vacuolar protein sorting events defined in a yeast sec18 (NSF) mutant. J. Cell Biol. *114*, 207–218.

Griff, I.C., Schekman, R., Rothman, J.E., and Kaiser, C.A. (1992). The yeast SEC17 gene product is functionally equivalent to mammalian α-SNAP protein. J. Biol. Chem. *267*, 12106–12115.

Grosse-Kunstleve, R.W.G., and Brunger, A.T. (1999). A highly automated heavy-atom search procedure for macromolecular structures. Acta Crystallogr. D, in press.

Groves, M.R., Hanlon, N., Turowski, P., Hemmings, B.A., and Barford, D. (1999). The structure of the protein phosphatase 2A PR65/A subunit reveals the conformation of its 15 tandemly repeated HEAT motifs. Cell *96*, 99–110.

Haas, A., and Wickner, W. (1996). Homotypic vacuolar fusion requires Sec17p (yeast α-SNAP) and Sec18p (yeast NSF). EMBO J. *15*, 3296–3305.

Halachmi, N., and Lev, Z. (1996). The Sec1 family: a novel family of proteins involved in synaptic transmission and general secretion. J. Neurochem. *66*, 889–897.

Hanson, P.I., Otto, H., Barton, N., and Jahn, R. (1995). The N-ethylmaleimide-sensitive fusion protein and α-SNAP induce a conformational change in syntaxin. J. Biol. Chem. *270*, 16955–16961.

Hanson, P.I., Roth, R., Morisaki, H., Jahn, R., and Heuser, J.E. (1997). Structure and conformational changes in NSF and its membrane receptor complexes visualized by quick-freeze/deep-etch electron microscopy. Cell *90*, 523–535.

Hayashi, T., Yamasaki, S., Nauenburg, S., Binz, T., and Niemann, H. (1995). Disassembly of the reconstituted synaptic vesicle membrane fusion complex in vitro. EMBO J. *14*, 2317–2325.

Hendrickson, W.A. (1985). Stereochemically restrained refinement of macromolecular structures. Methods Enzymol. *115*, 252–270.

Hohl, T.M., Parlati, F., Wimmer, C., Rothman, J.E., Söllner, T.H., and Engelhardt, H. (1998). Arrangement of subunits in 20S particles consisting of NSF, SNAPs, and SNARE complexes. Mol. Cell *2*, 539–548.

Holm, L., and Sander, C. (1993). Protein structure comparison by alignment of distance matrices (Dali 2.0). J. Mol. Biol. *233*, 123–138.

Huber, A.H., Nelson, W.J., and Weis, W.I. (1997). Three-dimensional structure of the armadillo repeat region of β-catenin. Cell *90*, 871–882.

Jiang, J.-S., and Brunger, A.T. (1994). Protein hydration observed by x-ray diffraction: solvation properties of penicillopepsin and neuraminidase crystal structures. J. Mol. Biol. *243*, 100–115.

Jones, T.A., Zou, J.Y., Cowan, S., and Kjeldgaard, M. (1991). Improved methods for building protein models in electron density maps and the location of errors in these models. Acta Crystallogr. A *47*, 110–119.

Jorgensen, W.L., and Tirado-Rives, J. (1988). The OPLS potential functions for protein energy minimizations for crystals of cyclic peptides and crambin. J. Am. Chem. Soc. *110*, 1657–1666.

Kee, Y., Lin, R.C., Hsu, S.-C., and Scheller, R.H. (1995). Distinct domains of syntaxin are required for synaptic vesicle fusion complex formation and dissociation. Neuron *14*, 991–998.

Kjeldgaard, M., Nissen, P., Thirup, S., and Nyborg, J. (1993). The crystal structure of elongation factor EF-Tu from *Thermus aquaticus* in the GTP conformation. Structure *1*, 35–50.

Kraulis, P. (1996). MOLSCRIPT: a program to produce both detailed and schematic plots of macromolecular structures. J. Appl. Crystallogr. *24*, 946–950.

Lamb, J.R., Tugendreich, S., and Hieter, P. (1995). Tetratricopeptide repeat interactions: to TPR or not to TPR? Trends Biochem. Sci. *20*, 257–259.

Leahy, D.J., Erickson, H.P., Aukhil, I., Joshi, P., and Hendrickson, W.A. (1994). Crystallization of a fragment of human fibronectin: introduction of methionine by site-directed mutagenesis to allow phasing via selenomethionine. Proteins *19*, 48–54.

Lenzen, C.U., Oppitz, D., Whiteheart, S.W., and Weis, W.I. (1998). Crystal structure of the hexamerization domain of N-ethylmaleimide-sensitive fusion protein. Cell *49*, 525–536.

Livingstone, C.D., and Barton, G.J. (1993). Protein sequence alignments: a strategy for the hierarchical analysis of residue conservation. Comput. Appl. Biosci. *9*, 745–756.

Malhotra, V., Orci, L., Glick, B.S., Block, M.R., and Rothman, J.E. (1988). Role of an N-ethylmaleimide-sensitive transport component in promoting fusion of transport vesicles with cisternae of the Golgi stack. Cell *54*, 83–94.

Mayer, A., Wickner, W., and Haas, A. (1996). Sec18p (NSF)-driven release of Sec17p (α-SNAP) can precede docking and fusion of yeast vacuoles. Cell *85*, 83–94.

Merritt, E.A., and Bacon, D.J. (1997). Raster 3D: photorealistic molecular graphics. Methods Enzymol. *277*, 505–524.

Miller, S., Janin, J., Lesk, A.M., and Chothia, C. (1987). Interior and surface of monomeric proteins. J. Mol. Biol. *196*, 641–656.

Nagiec, E.E., Bernstein, A., and Whiteheart, S.W. (1995). Each domain of the N-ethyl-maleimide-sensitive fusion protein contributes to its transport activity. J. Biol. Chem. *270*, 29182–29188.

Nicholls, A., Sharp, K.A., and Honig, B. (1991). Protein folding and association: insights from the interfacial and thermodynamic properties of hydrocarbons. Proteins *11*, 281–296.

Ordway, R.W., Pallanck, L., and Ganetzky, B. (1994). A TPR domain in the SNAP secretory proteins. Trends Biochem. Sci. *19*, 530–531.

Otto, H., Hanson, P.I., and Jahn, R. (1997). Assembly and disassembly of a ternary complex of synaptobrevin, syntaxin, and SNAP-25 in the membrane of synaptic vesicles. Proc. Natl. Acad. Sci. USA *94*, 6197–6201.

Otwinowski, Z., and Minor, W. (1997). Processing of X-ray data collected in oscillation mode. Methods Enzymol. *276*, 307–325.

Pannu, N.S., Murshdov, G.N., Dodson, E.J., and Read, R.J. (1998). Incorporation of prior phase information strengthens maximum likelihood structural refinement. Acta Crystallogr. D *54*, 1285–1294.

Poirier, M.A., Hao, J.C., Malkus, P.N., Chan, C., Moore, M.F., King, D.S., and Bennett, M.K. (1998). Protease resistance of syntaxin. SNAP-25. VAMP complexes. Implications for assembly and structure. J. Biol. Chem *273*, 11370–11377.

Rice, L.M., and Brunger, A.T. (1994). Torsion angle dynamics: reduced variable conformational sampling enhances crystallographic structure refinement. Proteins *19*, 277–290.

Rossi, G., Salminen, A., Rice, L.M., Brunger, A.T., and Brennwald, P. (1997). Analysis of a yeast SNARE complex reveals remarkable similarity to the neuronal SNARE complex and a novel function for the C terminus of the SNAP-25 homolog, Sec9. J. Biol. Chem. *272*, 16610–16617.

Rothman, J.E. (1994). Mechanisms of intracellular protein transport. Nature *372*, 55–63.

Schekman, R., and Orci, L. (1996). Coat proteins and vesicle budding. Science *271*, 1526–1533.

Schiavo, G., Gmachl, M.J., Stenbeck, G., Söllner, T.H., and Rothman, J.E. (1995). A possible docking and fusion particle for synaptic transmission. Nature *378*, 733–736.

Sikorski, R.S., Boguski, M.S., Goebl, M., and Hieter, P. (1990). A repeating amino acid motif in CDC23 defines a family of proteins and a new relationship among genes required for mitosis and RNA synthesis. Cell *60*, 307–317.

Söllner, T., Bennett, M.K., Whiteheart, S.W., Scheller, R.H., and Rothman, J.E. (1993). A protein assembly-disassembly pathway in vitro that may correspond to sequential steps of synaptic vesicle docking, activation, and fusion. Cell *75*, 409–418.

Sutton, R.B., Fasshauer, D., Jahn, R., and Brunger, A.T. (1998). Crystal structure of a SNARE complex involved in synaptic exocytosis at 2.4 Å resolution. Nature *395*, 347–353.

Tagaya, M., Wilson, D.W., Brunner, M., Arango, N., and Rothman, J.E. (1993). Domain structure of an N-ethyl-maleimide-sensitive fusion protein involved in vesicular transport. J. Biol. Chem. *268*, 2662–2666.

Thompson, J.D., Higgins, D.G., and Gibson, T.J. (1994). CLUSTAL W: improving the sensitivity of progressive multiple sequence alignment through sequence weighting, position-specific gap penalties and weight matrix choice. Nucleic Acids Res. *22*, 4673–4680.

Ungermann, C., Sato, K., and Wickner, W. (1998). Defining the function of trans-SNARE pairs. Nature *396*, 543–548.

Vetter, I.R., Arndt, A., Kutay, U., Görlich, D., and Wittinghofer, A. (1999). Structural view of the Ran-Importin β interaction at 2.3 Å resolution. Cell *97*, 635–646.

Weber, T., Zemelman, B.V., McNew, J.A., Westermann, B., Gmachl, M., Parlati, F., Söllner, T.H., and Rothman, J.E. (1998). SNAREpins: minimal machinery for membrane fusion. Cell *92*, 759–772.

Whiteheart, S.W., Brunner, M., Wilson, D.W., Wiedmann, M., Brunner, M., and Rothman, J.E. (1992). A multisubunit particle implicated in membrane fusion. J. Cell Biol. *117*, 531–538.

Yaffe, M.B., Rittinger, K., Volinia, S., Caron, P.R., Aitken, A., Leffers, H., Gamblin, S.J., Smerdon, S.J., and Cantley, L.C. (1997). The structural basis for 14-3-3:phosphopeptide binding specificity. Cell *91*, 961–971.

Yang, B., Gonzales, L., Prekeris, R., Steegmaier, M., Advani, R.J., and Scheller, R.H. (1999). SNARE interactions are not selective: implications for membrane fusion specificity. J. Biol. Chem. *274*, 5649–5653.

Ybe, J.A., Brodsky, F.M., Hofmann, K., Lin, K., Liu, S.-H., Chen, L., Earnest, T.N., Fletterick, R.J., and Hwang, P.K. (1999). Clathrin self-assembly is mediated by a tandemly repeated superhelix. Nature *399*, 371–375.

Yu, R.C., Hanson, P.I., Jahn, R., and Brunger, A.T. (1998). Structure of the ATP-dependent oligomerization domain of N-ethylmaleimide sensitive factor complexed with ATP. Nat. Struct. Biol. *5*, 803–811.

Yu, R.C., Jahn, R., and Brunger, A.T. (1999). NSF N-terminal domain crystal structure: models of NSF function. Mol. Cell *4*, this issue, 97–107.

Zhang, K.Y.J., and Main, P. (1990). Histogram matching as a new density modification technique for phase refinement and extension of protein molecules. Acta Crystallogr. A *46*, 41–46.

Protein Data Bank Accession Number

The accession number for the coordinates of the structure reported in this paper is 1QQE.